A First-Principles Analysis for Sulfur Tolerance of CeO_2 in Solid Oxide Fuel Cells

Hsin-Tsung Chen,[†] YongMan Choi,*[,‡] Meilin Liu,[‡] and M. C. Lin*[,†,§]

Department of Chemistry, Emory University, 1515 Dickey Drive, Atlanta, Georgia 30322, Center for Innovative Fuel Cell and Battery Technologies, School of Materials Science and Engineering, Georgia Institute of Technology, Atlanta, Georgia 30332, and Center for Interdisciplinary Molecular Science, National Chiao Tung University, Hsinchu, 30010, Taiwan

Received: January 23, 2007; In Final Form: April 4, 2007

The mechanism for $H_2S-CeO_2(111)$ interactions in solid oxide fuel cells (SOFCs) has been investigated by using periodic density functional theory (DFT) calculations. In order to properly characterize the effect of the localization of Ce_{4f} states on the interactions, DFT + U calculations were applied. Adsorption of H_2S, SH, and atomic S was initially examined to locate energetically favorable intermediates. The species adsorb favorably at the Ce-top, O-top, and Ce−O bridging sites, respectively. Potential energy profiles for the H_2S-CeO_2 (111) interactions along the three product channels producing H_2, H_2O, and SO_2 were constructed using the nudged elastic band (NEB) method. Calculations show that H_2S weakly bounds on $CeO_2(111)$ with a small binding energy, followed by dehydrogenation processes, forming surface sulfur species with an exothermicity of 29.9 kcal/mol. Molecular-level calculations demonstrated that the SO_2-forming pathway is energetically most favorable.

1. Introduction

Solid oxide fuel cells (SOFCs) have been attractive technologically because of their high-energy efficiency and the possibility of the direct utilization of a variety of fuels—natural gas, liquid fuels, gasified coal, and biofuels.[1−6] However, most of commercially available fuels contain small amounts of impurities such as sulfur-containing compounds that can degrade SOFC anodes.[7−11] Even though Ni/YSZ (yttria-stabilized zirconia; 8 mol % Y_2O_3) cermet anodes in SOFCs are very active to fuel oxidation, it is easily poisoned by low concentration of sulfur under SOFC operating conditions (600−1000 °C).[4,6] Therefore, it is very crucial to develop novel sulfur tolerant SOFC anodes with high catalytic activity. It is known that sulfur poisoning results from either the formation of atomic sulfur (S) or nickel sulfide (Ni_3S_2) through the decomposition of hydrogen sulfide (H_2S).[12] In recent years, various experimental studies[13−19] for the development of sulfur-tolerant anode materials have been reported. Choi and co-workers[20,21] computationally demonstrated that Cu-based anodes are more sulfur tolerant than Ni-based electrodes by comparing their adsorption energies.[22] Marquez et al.[23] reported that H_2 oxidation kinetics can be inhibited by H_2S addition using cluster-model approaches. Despite the high electrical conductivity and sulfur tolerance of Cu, it is not directly applicable for SOFCs due to its low catalytic ability toward fuel oxidation. He and co-workers recently reported that $Cu/CeO_2/YSZ$ cermet anodes can sustain up to 450 ppm of H_2S at 1073 K.[9] However, to the best of our knowledge, no molecular-level study on H_2S-CeO_2 interactions is available although understanding of the detailed mechanism of the interactions at the molecular level is very important. In this study, we elucidate the H_2S-CeO_2 interactions microscopically using periodic density functional theory (DFT). On the basis of energetically stable intermediate species for the interactions, detailed minimum-energy paths (MEPs) for all low-lying reaction pathways have been characterized and are reported herein.

2. Computational Methods

We applied DFT plane wave calculations as implemented in the Vienna *ab initio* simulation package (VASP) package[24,25] with the projector augmented wave method (PAW).[26] The generalized gradient approximation (GGA) with the Perdew−Wang 91 (PW91) exchange-correlation functional[27−29] was used. All the calculations were carried out using the Brillouim zone sampled with a (3 × 3 × 1) Monkhorst-Pack[30] mesh **k**-points grid, and a cutoff energy of 400 eV was used. It has been demonstrated[31−34] that DFT methods are not suitable for the study of reduced ceria due to the presence of the self-interaction error (SIE). Thus, in this study the DFT + U method[35] was applied in order to accurately correct the strong on-site Coulomb repulsion of Ce_{4f} states.[31−34,36] We used U and J of 7.0 and 0.7 eV, respectively, which are consistent with those reported by Jiang and co-workers.[37] For the surface model, we examined only $CeO_2(111)$ to characterize the H_2S-CeO_2 interactions because $CeO_2(111)$ is energetically the most stable[38−40] among the low-index $CeO_2(111)$, (110), and (100) surfaces. As shown in Figure 1, the CeO_2 (111) surface model with 12 atomic layers—a p($\sqrt{3} \times 2$) lateral cell—was constructed. The bottom six layers of the surface model were fixed to the estimated bulk parameters, while the remaining layers were fully optimized. A vacuum space greater than 15 Å was introduced to prevent interactions between slabs. The adsorption energies were calculated by $\Delta E_{ads} = E[\text{surface−adsorbate}] - E[\text{surface}] - E[\text{adsorbate}]$, where E[surface−adsorbate], E[surface], and E[adsorbate] are the calculated electronic energies of adsorbed species on $CeO_2(111)$, bare $CeO_2(111)$, and free H_2S, SH, or S, respectively. The nudged elastic band (NEB) method[41,42] was

* Corresponding authors. Tel: +1-404-727-2825. Fax: +1-404-727-6586. E-mail: chemmcl@emory.edu; yongman.choi@mse.gatech.edu.
[†] Emory University.
[‡] Georgia Institute of Technology.
[§] National Chiao Tung University.

10.1021/jp0705774 CCC: $37.00
Published on Web 07/04/2007

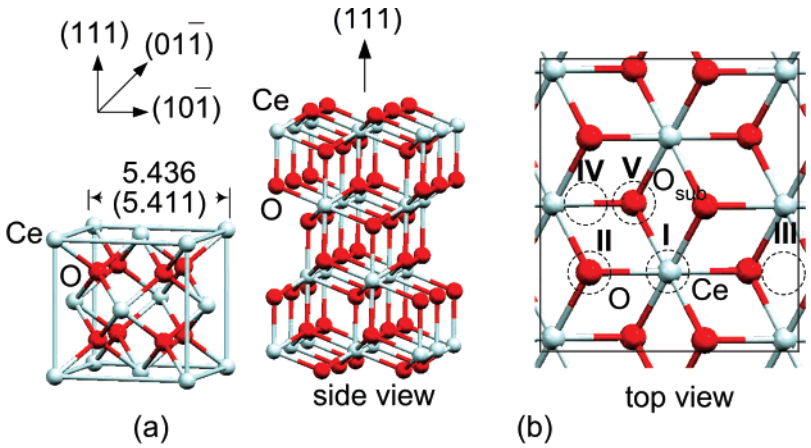

Figure 1. (a) The fluorite crystal structure of CeO_2. The lattice constant in parenthesis represents an experimental value in Å. (b) Side and top views of the CeO_2 (111) surface model. **I**, **II**, **III**, **IV**, and **V** correspond to active sites for "Ce-top", "O-top", "Ce−Ce bridge", "O−O bridge", and "O_{sub}-top" sites, respectively. O_{sub} denotes oxygen anions on the second layer. A rectangle represents the supercell used in this study.

TABLE 1: Geometrical Parameters and Vibrational Frequencies of H_2S, SH, H_2, H_2O, and SO_2 Calculated at the GGA-PAW Level

	H_2S		SH		H_2		H_2O		SO_2	
	calcd	expt[a]	calcd	expt[b]	calcd	expt[c]	calcd	expt[d]	calcd	expt[e]
r(S−H, H−H, O−H or S−O) (Å)	1.345	1.328	1.349	1.346	0.743	0.740	0.957	0.958	1.454	1.432
θ(H−X−H or O−S−O) (deg)	90.5	91.6					104.5	104.5	119.5	119.3
υ_{asym} (cm^{-1})	2669	2628	2675	2660			3856	3756	1282	1360
υ_{sym} (cm^{-1})	2649	2615			4435	4400	3741	3657	1091	1151
γ_{bend} (cm^{-1})	1163	1183					1585	1595	488	518

[a−e] Correspond to refs 43, 44, 45, 46 and 47, and 48 and 49, respectively.

applied to map out MEPs after locating plausible local minima. All transition states were verified by the number of imaginary frequencies (NIMG) with NIMG = 1. Complied in Table 1 are geometrical parameters and vibrational frequencies of H_2S, SH, H_2, H_2O and SO_2 computed in a 15 Å cubic box, which are in good agreement with available literature values.

3. Results and Discussion

Plausible intermediates for the H_2S-CeO_2 interactions were initially optimized by placing H_2S, SH, or S species at five different active sites on the (111) surface, including "Ce-top", "O-top", "Ce−Ce bridge", "O−O bridge", and "O_{sub}-top", corresponding to **I**, **II**, **III**, **IV**, and **V**, respectively, as illustrated in Figure 1b. All optimized structures are presented in Figures 2 and S1. Table 2 displays the adsorption energies and geometric parameters of adsorbed H_2S, SH, and S on the CeO_2 (111) surface. Furthermore, to examine the difference between DFT and DFT + U methods, we compared structures and energetics as compiled in Table 2. The adsorption-energy calculations demonstrate that the effects from DFT and DFT + U calculations for the intermediates adsorbed on partially reduced ceria surfaces are significant, while those on perfect CeO_2 for molecular H_2S adsorption are negligible (<0.3 kcal/mol). In the following, we will discuss the mechanistic details based on the DFT + U results.

3.1. Adsorption of H_2S, SH, S, and H on CeO_2(111). *H_2S Adsorption.* Shown in Figure 2 are the optimized intermediates for H_2S adsorption with hydrogen up, down, or parallel to the surface. Table 2 gives geometrical information and adsorption energies for stable configurations. The calculated energies of adsorbed H_2S species (**I**-H_2S-u-p, **I**-H_2S-p [LM1], and **IV**-H_2S-d) are close to the average bond energy errors of the GGA method (~2.0 kcal/mol).[50] However, we assumed that they are weakly bound intermediates on the surface via molecular

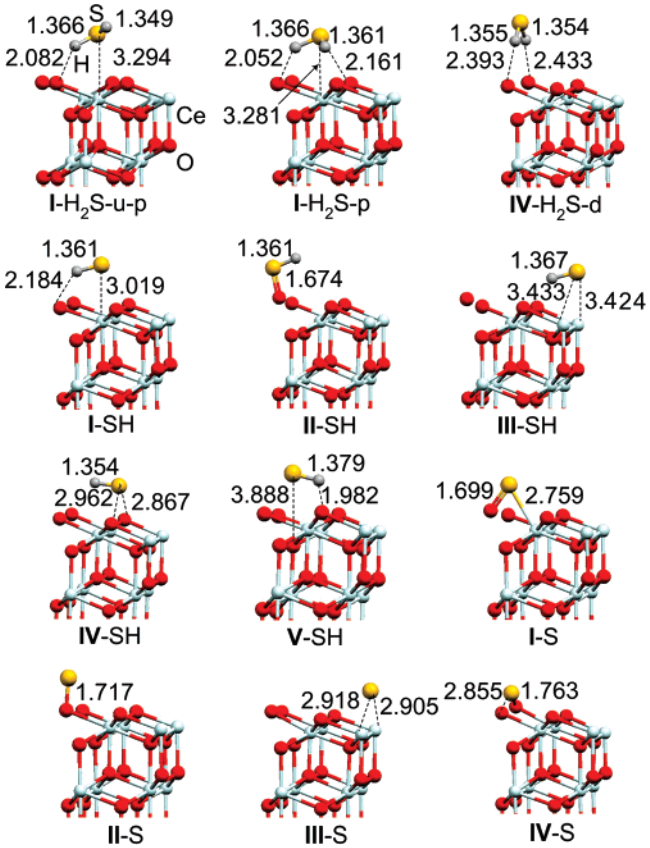

Figure 2. Optimized geometries of adsorbed H_2S, SH, and atomic S on CeO_2(111) at the DFT + U level.

adsorption and connectable to chemisorbed species even though the DFT method used in this study may not be suitable to describe van der Waals interactions.[51] A variety of energetically

TABLE 2: Optimized Structural Parameters and Adsorption Energies of H_2S, SH, and S Species on CeO_2(111) Calculated Using DFT and DFT[c] + U Methods

species	S−M[a] (Å)	S−H (Å)	ΔE_{ads} (kcal/mol)
		H_2S Adsorption	
I-H_2S-u-p	3.269 (3.275)	1.366, 1.349 (1.362, 1.345)	−2.8 (−2.7)
I-H_2S-p [LM1][b]	2.470 (2.498)	1.366, 1.361 (1.362, 1.359)	−3.5 (−3.8)
IV-H_2S-d	3.172 (3.261)	1.355, 1.354 (1.354, 1.353)	−2.1 (−1.8)
		SH Adsorption	
I-SH	2.233 (2.278)	1.361 (1.357)	−9.0 (−6.9)
II-SH	1.646 (1.664)	1.361 (1.359)	−34.4 (−35.7)
III-SH	1.568 (1.667)	1.367 (1.370)	−32.0 (−31.1)
IV-SH	2.005 (1.982)	1.354 (1.356)	−6.0 (−3.6)
V-SH	2.234 (2.095)	1.369 (1.362)	−2.3 (−2.8)
		S Adsorption	
I-S	1.383 (1.342)		−54.5 (−71.1)
II-S	1.717 (1.684)		−46.1 (−64.8)
III-S	1.186 (1.189)		−52.2 (−67.8)
IV-S	1.028 (0.983)		−42.5 (−44.6)

[a] The shortest distance between adsorbed species and the CeO_2 surface. [b] It is used for the mechanistic studies. [c] Those calculated by the DFT method are in parentheses.

unstable intermediates are shown in Table S1 and Figure S1 in the Supporting Information. For brevity, "u", "d", and "p" denote hydrogen up, down, and parallel to the surface, respectively. As summarized in Table 2, the **I**-H_2S-p configuration is the most stable with an adsorption energy of −3.5 kcal/mol, similar to a previous study[52] on H_2O−CeO_2(111) interactions. The distances between the S atom and the surface of **I**-H_2S-u-p, **I**-H_2S-p, and **IV**-H_2S-d are 3.269, 2.470, and 3.172 Å, respectively. All the configurations parallel to the surface, **I**-H_2S-p, **II**-H_2S-p, **III**-H_2S-p, **IV**-H_2S-p, and **V**-H_2S-p, are slightly tilted by approximately 30−45° from the surface.

SH, S, and H Adsorption. Similar to the H_2S adsorption, in order to carry out mechanistic studies, we examined the adsorption sites and energies for SH, S, and H on CeO_2(111). Figures 2 and S3 display side and top views of optimized local minima of the SH species on CeO_2 (111). Their adsorption energies and geometrical parameters are summarized in Table 2. While H_2S preferentially adsorbs on the Ce-top site, the most stable configuration for SH adsorption is located at the O-top site. For the **II**-SH and **III**-SH structures with adsorption energies of −34.4 and −32.0 kcal/mol, respectively, their S atom is bound to an O anion of the surface with their S−O distance of 1.674 and 1.681 Å, respectively. Due to the strong overlaps between p orbitals of the S atom and surface O anions, the S−O covalent bonds result in higher absorption energies compared to those of **I**-SH, **IV**-SH, and **V**-SH (−9.0, −6.0, and −2.3 kcal/mol, respectively). In addition, the strong S−O bond produces much relaxation of the surface, especially for the surface O anions bonded to the sulfur atoms, resulting in the protrusion by approximately 0.37−0.43 Å from the surface. The Ce−S bond length of **I**-SH (3.019 Å) is slightly shorter than that of **I**-H_2S-p for H_2S adsorption (3.281 Å).

For S adsorption, the S atom which is placed on the Ce-top site (**I**-S) diffuses to a Ce−O bridge site as shown in Figures 2 and S3. Table 2 shows that **I**-S with the adsorption energy of −54.5 kcal/mol is the most stable, while **II**-S, **III**-S, and **IV**-S have the energies of −46.1, −52.2, and −42.5 kcal/mol, respectively. While the S−O distances of **I**-S, **II**-S, **III**-S, and **IV**-S are 1.699, 1.717, 1.716, and 1.763 Å, the Ce−S distances are 2.759, 3.299, 2.918, and 3.374 Å, respectively. Similar to the SH adsorption, the surface O anions bonded to sulfur atoms move upward by approximately 0.13−0.35 Å.

Regarding H adsorption, we optimized two configurations on the Ce- and O-top sites. Similar to a recent theoretical result by Vicario and co-workers,[53] the H atom adsorbs preferentially on the O-top site with an absorption energy and O−H distance of −78.7 kcal/mol and 0.973 Å, respectively, which are in agreement with their results of −82.1 kcal/mol and 0.97 Å, respectively.

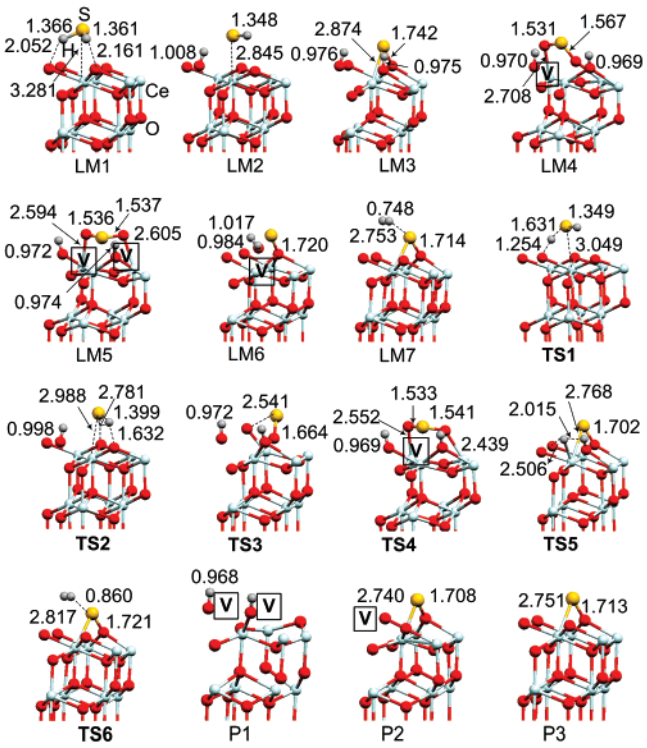

Figure 3. Geometrical illustration of intermediates, transition states, and products for the H_2S−CeO_2 interactions at the DFT + U level.

3.2. Reaction Mechanism of H_2S-CeO_2(111) Interactions. To characterize probable reaction pathways of the H_2S adsorption/decomposition processes on the CeO_2(111) surface, we applied energetically the most stable configurations obtained from the H_2S, SH, and S adsorption (**I**-H_2S-p, **I**-SH, and **I**-S, respectively) to map out the MEPs using the NEB method by connecting the local minima. Figure 3 shows the optimized structures of intermediates, transition states, and products, while Figure 4 represents schematic potential energy profiles based on the NEB calculations. As shown in Figure 4, H_2S initially adsorbs on the surface without a tight transition state, producing LM1 with an exothermicity of 3.5 kcal/mol, followed by the

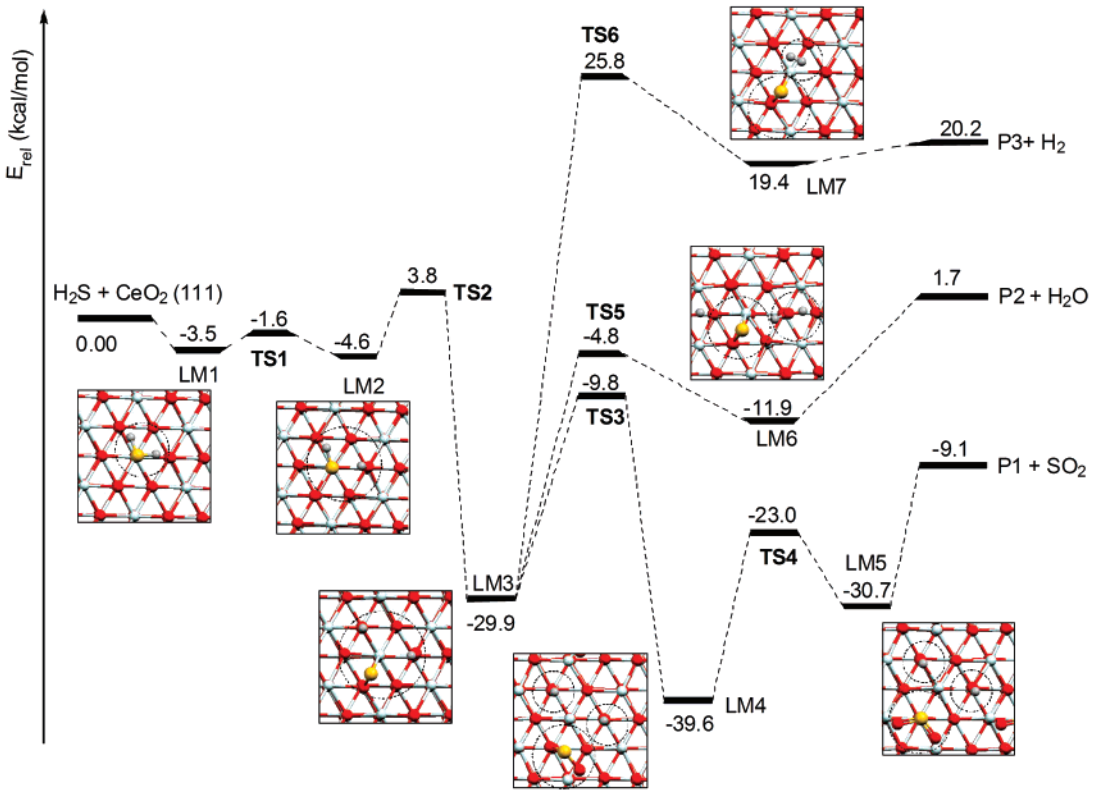

Figure 4. Schematic potential energy profiles for the H_2S-CeO_2 interactions at 0 K at the DFT + U level.

TABLE 3: Summary of Estimated Vibrational Frequencies of Intermediates from the H_2S-CeO_2 Interactions

intermediate	surface species	ν (cm^{-1})	surface species	ν (cm^{-1})
LM1	H_2S	2511, 2451, 1226		
LM2	SH, $SCe_{surface}$	2662, 887	OH	2917
LM3	$SO_{surface}$	637	OH	3595, 3551
LM4	SO, $SO_{surface}$	957, 556	OH	3651, 3578
LM5	SO_2	989, 907, 436	OH	3456, 3322
LM6	$SO_{surface}$	744, 607	H_2O	3582, 2871, 1561
LM7	$SO_{surface}$	401	H_2	4344

first dehydrogenation process ($H_2S \rightarrow SH + H$). The dissociating H atom initially diffuses to an adjacent surface O anion forming an O−H bond via **TS1** with a reaction barrier of 1.9 kcal/mol. The Ce−S bond length of the transition state **TS1** is shortened by approximately 0.232 Å compared to that of the molecularly adsorbed H_2S, LM1 (3.281 and 3.049 and Å, respectively). The breaking H−S and forming O−H bonds at **TS1** are 1.631 and 1.254 Å, respectively. Then the second dehydrogenation step takes place ($SH \rightarrow S + H$), by overcoming an 8.4 kcal/mol reaction barrier at **TS2,** producing LM3 with a reaction energy of 25.3 kcal/mol compared to LM2. At the transition state **TS2**, the S atom moves to an adjacent O atom to form an S−O bond of 2.781 Å—locating at the Ce−O bridge site with an S−Ce bond of 2.988 Å (see the top view in Figure S4), whereas the breaking S−H and forming O−H bonds are 1.399 and 1.632 Å, respectively.

According to previous studies[54,55] for the electrochemical reaction of H_2S on Ni/YSZ, an SO_2-forming process is thermodynamically the most probable under SOFC conditions, implying that the surface adsorbates formed from the H_2S-CeO_2 interactions can further react with oxygen anions (O^{2-}). After the dehydrogenation reactions, a reaction pathway can take place by overcoming a 20.1 kcal/mol reaction barrier at **TS3** with an S−O bond of 2.541 Å, producing LM4 and an oxygen vacancy with 39.6 kcal/mol exthothermicity. Then, an oxygen anion from the surface can react with the SO species of LM4, generating LM5 with an SO_2 surface species and two oxygen vacancies via **TS4** with a reaction barrier of 16.6 kcal/mol. The S−O bond lengths of LM5 are 1.537 and 1.536 Å, which are slightly longer than that of free SO_2. (1.454 Å, see Table 1). Further elongation of the Ce−S bond of LM5 produces the $SO_2 + CeO_{2-x}$ (P1) products without a well-defined reaction barrier. The overall reaction energy for the formation of SO_2 + P1 is exothermic by 9.1 kcal/mol. In addition, as shown in Figure 4, two $H-O_{surface}$ species of the LM3 intermediate can undergo H-migration via **TS5** with a reaction barrier of 25.1 kcal/mol, leading to the H_2O-containing LM6 intermediate with an endothermicty of 18.0 kcal/mol. Forming and breaking O−H bonds in **TS5** are 2.015 and 2.506 Å, respectively. Due to the formation of an H_2O species along with the reduction of Ce^{4+} to Ce^{3+}, an oxygen vacancy is generated, followed by barrierless H_2O desorption from LM6. The process produces the non-stoichiometric CeO_2 (P2) with the adsorbed S species and an oxygen vacancy. An overall endothermicity of this process is only 1.7 kcal/mol. As presented in Figure 4, the OH-containing LM3 intermediate can undergo an H_2-forming process giving LM7 via **TS6** with a reaction barrier of 55.7 kcal/mol; this suggests that the H_2-elimination pathway is less favorable than the two processes. The weakly bound H_2 species of LM7 can barrierlessly desorb to produce $H_2 + CeO_2S$ (P3) with an endothermicity of 20.2 kcal/mol. Under SOFC operating conditions, formation of H_2O instead of H_2 is more

likely. The result of this molecular-level study indicates that the SO_2-forming process is the most probable reaction pathway from the H_2S-CeO_2 interaction. To simulate the H_2S-CeO_2 interactions under SOFC operating conditions, molecular dynamics (MD) simulations will be carried out in a future study.

In addition to the mechanistic studies, in order to guide a future surface vibrational spectroscopic study, the vibrational frequencies for the adsorbed species on the CeO_2 (111) surface were estimated as summarized in Table 3. The calculated frequencies of LM1 with 2511, 2451, and 1226 cm^{-1} are assigned to asymmetric, symmetric, and bend modes of adsorbed H_2S species, respectively. Comparing with the experimental and calculated frequencies of gas-phase H_2S summarized in Table 1, the vibrational frequencies of the adsorbed H_2S species red-shifted, resulting from weakening of the S−H bonds. The predicted vibrational frequencies of LM2 at 2917, 2662, and 887 cm^{-1} are attributed to O−H, S−H, and $S-Ce_{surfce}$ stretching modes based on our normal-mode analysis. The much lower O−H vibration frequency of LM2 (2917 cm^{-1}) than the experimental value[56−58] of 3600 cm^{-1} may result from the presence of a weak H···S bonding (−OH···SH−) in LM2. On the other hand, the predicted O−H frequencies of LM3 and LM4 (3595 and 3551 cm^{-1} and 3651 and 3578 cm^{-1}, respectively) are in close agreement with the experimental value, 3600 cm^{-1}. The vibration mode of LM3 at 637 cm^{-1} is attributable to the S-surface vibration, whereas those of LM4 at 957 and 556 cm^{-1} may be attributed to S−O and S-surface vibrations, respectively. The reduction of Ce cations and the formation of oxygen vacancies slightly alter the O−H vibrational mode of LM5 and LM3 (3456 and 3322 cm^{-1} and 3595 and 3551 cm^{-1}, respectively). The estimated vibrational frequencies of LM5 at 989, 907 and 436 cm^{-1} are assigned to asymmetric, symmetric, and bend modes of the adsorbed SO_2 species. The calculated frequencies of H_2O species of LM6 (3582, 2871, and 1561 cm^{-1}) are similar to those of H-bonded H_2O species (3686, 3140, and 1640 cm^{-1}),[59] while those at 744 and 607 cm^{-1} are related to S-surface vibration modes. For LM7, its H−H stretching mode with 4344 cm^{-1} is close to that of gas-phase H_2 as compiled in Table 1, implying that LM7 has the characteristics of the products and the 401 cm^{-1} may be assigned to the S-surface vibration mode.

4. Conclusion

The interactions of H_2S with CeO_2(111) have been elucidated using periodic DFT calculations. Three types of sulfur-containing species (H_2S, SH, and atomic S) were initially employed to locate plausible intermediates. It was found that H_2S, SH, and S preferentially adsorb on the Ce-top, O-top, Ce−O bridge sites with adsorption energies of −3.5, −34.4, and −54.5 kcal/mol, respectively. PESs for the H_2S/CeO_2 (111) interactions have been constructed. The reaction barriers of the H_2S dehydrogenation processes producing SH + H and S + 2H are quite small, 1.9 and 8.4 kcal/mol, respectively, while their exothermicities are −4.6 and −29.9 kcal/mol, respectively. In addition, the surface adsorbates formed through the dehydrogenation processes can further react with oxygen anions (O^{2-}), producing H_2O and SO_2 under SOFC operating conditions. According to our MEP calculations, the SO_2-forming pathway may be the key product channel, similar to the previous studies[54,55] for the electrochemical reaction of H_2S on Ni/YSZ. Furthermore, the vibrational frequencies of the intermediate species were estimated to guide future surface vibrational spectroscopic studies.

Acknowledgment. We acknowledge the use of CPU's from the National Center for High-performance Computing, Taiwan, supported by INER under Contract No. NL 940251. M.C.L. also wants to acknowledge support from the MOE ATP program, Taiwan Semiconductor Manufacturing Co. for the TSMC Distinguished Professorship and the Taiwan National Science Council for the Distinguished Visiting Professorship at the Center for Interdisciplinary Molecular Science, National Chiao Tung University, Hsinchu, Taiwan. This work was supported by the U.S. DOE SECA Coal Technology Program under Grant No. DE-FC26-04NT42219.

Supporting Information Available: TABLE S1 compiles structural parameters and adsorption energies from H_2S Adsorption on CeO_2(111). Figure S1 illustrates optimized geometries of adsorbed H_2S species at various sites on CeO_2(111). Figures S2 and S3 show top views of adsorbed H_2S and SH and S species, respectively, on CeO_2(111). Figure S4 are top views of intermediates and transition states for the H_2S-CeO_2 (111) interactions. This material is available free of charge via the Internet at http://pubs.acs.org.

References and Notes

(1) Atkinson, A.; Barnett, S.; Gorte, R. J.; Irvine, J. T. S.; McEvoy, A. J.; Mogensen, M.; Singhal, S. C.; Vohs, J. *Nat. Mater.* **2004**, *3*, 17.
(2) Minh, N. Q. *J. Am. Ceram. Soc.* **1993**, *76*, 563.
(3) Minh, N. Q. *Solid State Ionics* **2004**, *174*, 271.
(4) Minh, N. Q.; Takahashi, T. *Science and Technology of Ceramic Fuel Cells*; Elsevier Science: Amsterdam, 1995.
(5) Singh, P.; Minh, N. Q. *Int. J. Appl. Ceram. Technol.* **2004**, *1*, 5.
(6) Singhal, S. C.; Kendall, K. *High-temperature Solid Oxide Fuel Cells: Fundamentals, Design and Applications*; Elsevier Science: Amsterdam, 2003.
(7) Bartholomew, C. H. *Appl. Catal., A* **2001**, *212*, 17.
(8) Bartholomew, C. H.; Agrawal, P. K.; Katzer, J. R. *Adv. Catal.* **1982**, *31*, 135.
(9) He, H. P.; Gorte, R. J.; Vohs, J. M. *Electrochem. Solid-State Lett.* **2005**, *8*, A279.
(10) Kim, H.; Vohs, J. M.; Gorte, R. J. *Chem. Commun.* **2001**, *22*, 2334.
(11) Marianowski, L. G.; Anderson, G. L.; Camara, E. H. US Patent 5071718, 1988.
(12) Roberts, M. W.; McKee, C. S. *Chemistry of the Metal-Gas Interface*; Clarendon Press: Oxford, 1978.
(13) Aguilar, L.; Zha, S. W.; Cheng, Z.; Winnick, J.; Liu, M. *J. Power Sources* **2004**, *135*, 17.
(14) Aguilar, L.; Zha, S. W.; Li, S. W.; Winnick, J.; Liu, M. *Electrochem. Solid-State Lett.* **2004**, *7*, A324.
(15) Cheng, Z.; Zha, S. W.; Aguilar, L.; Wang, D.; Winnick, J.; Liu, M. *Electrochem. Solid-State Lett.* **2006**, *9*, A31.
(16) Cheng, Z.; Zha, S. W.; Liu, M. *J. Electrochem. Soc.* **2006**, *153*, A1302.
(17) Zha, S. W.; Cheng, Z.; Liu, M. *Electrochem. Solid-State Lett.* **2005**, *8*, A406.
(18) Zha, S. W.; Tsang, P.; Cheng, Z.; Liu, M. *J. Solid State Chem.* **2005**, *178*, 1844.
(19) Zha, S.; Cheng, Z.; Liu, M. *J. Electrochem. Soc.* **2007**, *154*, B201.
(20) Choi, Y. M.; Compson, C.; Lin, M. C.; Liu, M. *Chem. Phys. Lett.* **2006**, *421*, 179.
(21) Choi, Y. M.; Compson, C.; Lin, M. C.; Liu, M. *J. Alloys Compd.* **2007**, *427*, 25.
(22) Predicted adsorption energies of atomic sulfur (S) on relaxed fcc Ni(111) and Cu(111) surfaces are 125 and 101 kcal/mol, respectively, while those of H_2S on the Ni(111) and Cu(111) surfaces are 8.1 and ∼0.0 kcal/mol, respectively.
(23) Marquez, A. I.; De Abreu, Y.; Botte, G. G. *Electrochem. Solid-State Lett.* **2006**, *9*, A163.
(24) Kresse, G.; Hafner, J. *Phys. Rev. B* **1993**, *47*, 558.
(25) Kresse, G.; Furthmüller, J. *Phys. Rev. B* **1996**, *54*, 11169.
(26) Blöchl, P. E. *Phys. Rev. B* **1994**, *50*, 17953.
(27) Perdew, J. P.; Burke, K.; Ernzerhof, M. *Phys. Rev. Lett.* **1996**, *77*, 3865.
(28) Perdew, J. P.; Chevary, J. A.; Vosko, S. H.; Jackson, K. A.; Pederson, M. R.; Singh, D. J.; Fiolhais, C. *Phys. Rev. B* **1992**, *46*, 6671.
(29) Perdew, J. P.; Wang, Y. *Phys. Rev. B* **1992**, *45*, 13244.
(30) Monkhorst, H. J.; Pack, J. D. *Phys. Rev. B* **1976**, *13*, 5188.
(31) Nolan, M.; Grigoleit, S.; Sayle, D. C.; Parker, S. C.; Watson, G. W. *Surf. Sci.* **2005**, *576*, 217.
(32) Nolan, M.; Parker, S. C.; Watson, G. W. *Surf. Sci.* **2005**, *595*, 223.

(33) Fabris, S.; de Gironcoli, S.; Baroni, S.; Vicario, G.; Balducci, G. *Phys. Rev. B* **2005**, *71*, 041102.

(34) Fabris, S.; Vicario, G.; Balducci, G.; de Gironcoli, S.; Baroni, S. *J. Phys. Chem. B* **2005**, *109*, 22860.

(35) Dudarev, S. L.; Botton, G. A.; Savrasov, S. Y.; Humphreys, C. J.; Sutton, A. P. *Phys. Rev. B* **1998**, *57*, 1505.

(36) Chen, H.-T.; Choi, Y. M.; Liu, M.; Lin, M. C. *Chem. Phys. Chem.* **2007**, *8*, 849.

(37) Jiang, Y.; Adams, J. B.; Schilfgaarde, M. V. *J. Chem. Phys.* **2005**, *123*, 064701.

(38) Yang, Z. X.; Woo, T. K.; Baudin, M.; Hermansson, K. *J. Chem. Phys.* **2004**, *120*, 7741.

(39) Lyons, D. M.; Ryan, K. M.; Morris, M. A. *J. Mater. Chem.* **2002**, *12*, 1207.

(40) Lyons, D. M.; McGrath, J. P.; Morris, M. A. *J. Phys. Chem. B* **2003**, *107*, 4607.

(41) Mills, G.; Jönsson, H.; Schenter, G. *Surf. Sci.* **1995**, *324*, 305.

(42) Henkelman, G.; Uberuaga, B. P.; Jönsson, H. *J. Chem. Phys.* **2000**, *113*, 9901.

(43) Herzberg, G. *Molecular Spectra and Molecular Structure Electronic Spectra and Electronic Structure of Polyatomic Molecules*; Van Nostrand: New York, 1966; Vol. III.

(44) Huber, K. P.; Herzberg, G. *Molecular Spectra and Molecular Structure Constants of Diatomic Molecules*; Van Nostrand: New York, 1979; Vol. IV.

(45) *CRC Handbook of Chemistry and Physics*, 76th ed.; CRC Press: New York, 1996.

(46) Hoy, A. R.; Bunker, P. R. *J. Mol. Spectrosc.* **1979**, *74*, 1.

(47) Benedict, W. S.; Gailar, N.; Plyler, E. K. *J. Chem. Phys.* **1956**, *24*, 1139.

(48) Barker, E. F. *Rev. Mod. Phys.* **1942**, *14*, 0202.

(49) Kivelson, D. *J. Chem. Phys.* **1954**, *22*, 904.

(50) Kohn, W.; Becke, A. D.; Parr, R. G. *J. Phys. Chem.* **1996**, *100*, 12974.

(51) Kristyán, S.; Pulay, P. *Chem. Phys. Lett.* **1994**, *229*, 175.

(52) Henderson, M. A.; Perkins, C. L.; Engelhard, M. H.; Thevuthasan, S.; Peden, C. H. F. *Surf. Sci.* **2003**, *526*, 1.

(53) Vicario, G.; Balducci, G.; Fabris, S.; de Gironcoli, S.; Baroni, S. *J. Phys. Chem. B* **2006**, *110*, 19380.

(54) Yentekakis, I. V.; Vayenas, C. G. *J. Electrochem. Soc.* **1989**, *136*, 996.

(55) Peterson, D. R.; Winnick, J. *J. Electrochem. Soc.* **1998**, *145*, 1449.

(56) Badri, A.; Binet, C.; Lavalley, J. C. *J. Chem. Soc., Faraday Trans.* **1996**, *92*, 4669.

(57) Binet, C.; Daturi, M.; Lavalley, J. C. *Catal. Today* **1999**, *50*, 207.

(58) Laachir, A.; Perrichon, V.; Badri, A.; Lamotte, J.; Catherine, E.; Lavalley, J. C.; El Fallah, J.; Hilaire, L.; Le Normand, F.; Quéméré, E.; Sauvion, G. N.; Touret, O. *J. Chem. Soc., Faraday Trans.* **1991**, *87*, 1601.

(59) Daturi, M.; Finocchio, E.; Binet, C.; Lavalley, J. C.; Fally, F.; Perrichon, V. *J. Phys. Chem. B* **1999**, *103*, 4884.